Journal of
Applied
Crystallography

ISSN 0021-8898

Received 14 May 2013
Accepted 13 August 2013

Temperature dependence of ion track formation in quartz and apatite

D. Schauries,[a]* M. Lang,[b] O. H. Pakarinen,[c] S. Botis,[b] B. Afra,[a] M. D. Rodriguez,[a] F. Djurabekova,[c] K. Nordlund,[c] D. Severin,[d] M. Bender,[d] W. X. Li,[b] C. Trautmann,[d,e] R. C. Ewing,[b] N. Kirby[f] and P. Kluth[a]

[a]Department of Electronic Materials Engineering, Research School of Physics and Engineering, The Australian National University, Canberra, ACT 0200, Australia, [b]Department of Earth and Environmental Sciences, University of Michigan, Ann Arbor, MI 48109, USA, [c]Division of Materials Physics, Department of Physics, University of Helsinki, 00014 Helsinki, Finland, [d]GSI Helmholtz Centre for Heavy Ion Research, Planckstrasse 1, 64291 Darmstadt, Germany, [e]Technische Universität Darmstadt, 64287 Darmstadt, Germany, and [f]Australian Synchrotron, 800 Blackburn Road, Clayton, VIC 3168, Australia. Correspondence e-mail: daniel.schauries@anu.edu.au

Ion tracks were created in natural quartz and fluorapatite from Durango, Mexico, by irradiation with 2.2 GeV Au ions at elevated temperatures of up to 913 K. The track radii were analysed using small-angle X-ray scattering, revealing an increase in the ion track radius of approximately 0.1 nm per 100 K increase in irradiation temperature. Molecular dynamics simulations and thermal spike calculations are in good agreement with these values and indicate that the increase in track radii at elevated irradiation temperatures is due to a lower energy required to reach melting of the material. The post-irradiation annealing behaviour studied for apatite remained unchanged.

1. Introduction

Ion tracks are narrow cylindrical regions of high-defect density that are a few nanometres in diameter and up to tens of micrometres in length that result from the interaction of high-energy heavy ions with the electrons of a target material. Ion tracks are of high interest in a wide range of applications in materials science and nanotechnology, nuclear physics, geo- and thermochronology, archaeology, and interplanetary science. In nature, these tracks occur in minerals such as apatite and zircon as a result of the fission of incorporated traces of ^{238}U. Tracks of fission fragments are used for determining the age and thermal history of geological samples (Silk & Barnes, 1959; Wagner & Van den Haute, 1992; Gallagher *et al.*, 1998). They provide information useful for the modelling of sedimentary basins and long-term continental denudation (Reiners & Shuster, 2009). Fission track (FT) dating generally utilizes chemical etching to dissolve the damaged material and enlarge the tracks, converting them into open channels that can be imaged by optical microscopy. The drawback of the etching process is that it completely erases the initial damage structure of the tracks (Price & Walker, 1962). This limits the understanding of the primary damage morphology and its dependence on geological parameters, which is important for an accurate interpretation of the distribution of etched fission tracks.

Typical characterization techniques to study unetched tracks are transmission electron microscopy (TEM) (Paul & Fitzgerald, 1992; Meftah *et al.*, 1994; Li *et al.*, 2012) and Rutherford backscattering spectrometry (Villa *et al.*, 1999). We have recently shown that small-angle X-ray scattering (SAXS) is a powerful tool to study ion tracks (Kluth, Schnohr, Sprouster *et al.*, 2008; Kluth, Schnohr, Pakarinen *et al.*, 2008), well suited for tracks in minerals such as quartz (Afra *et al.*, 2013) and apatite (Afra *et al.*, 2011).

When investigating the thermal history of geological samples, the annealing behaviour of fission tracks is commonly studied using chemical etching. Heat leads to defect annealing and typically results in a shortening of the etchable length of the tracks (Gleadow *et al.*, 1986). Such experiments consider how heat affects existing tracks, but ignores a possible influence of the temperature during the track formation process itself. Fission tracks are known to be formed and retained under elevated temperatures, *e.g.* up to 400 K in apatite (Gallagher *et al.*, 1998; Gleadow *et al.*, 1986) and up to 500 K in zircon (Bernet & Garver, 2005). The question of whether the track morphology and the damage cross section depend on the irradiation temperature has not yet been addressed for amorphizable materials such as apatite and quartz, as pointed out in a recent review article (Klaumünzer, 2004). For non-amorphous tracks in LiF, an investigation by Schwartz *et al.* (2001) demonstrated that the track size increases as a function of irradiation temperature, and Kamarou *et al.* (2006) showed that ion tracks in InP, formed at room temperature (RT), are larger than those formed at liquid nitrogen temperature.

Here, we demonstrate that elevated temperatures during high-energy irradiation with predominant electronic stopping in quartz and fluorapatite lead to an increase in damage cross section for both materials. The situation is quite different from

irradiation with low-energy ions where ballistic stopping is predominant. Elevated irradiation temperatures generally lead to dynamic annealing of defects and thus reduced defect concentrations (Dhar *et al.*, 1999). As a result, the amorphization threshold increases with increasing irradiation temperature. The subject may have implications not only for fission track dating but also for the resistance of materials in extreme environments, with exposure to highly energetic particles.

2. Methods

Natural crystalline quartz and fluorapatite from Durango, Mexico, were polished down to a thickness of approximately 200 µm. Apatite was cut perpendicular, quartz perpendicular and parallel to the *c* axis. In order to remove pre-existing natural tracks and other defects, all specimens were annealed at 773 K for 24 h. Apatite from Durango was chosen as it is commonly used as a standard for FT studies (Gallagher *et al.*, 1998). Quartz does not have a direct relevance for FT studies. However, its comparatively simple structure provides a model system for silicate materials and is accessible by molecular dynamics (MD) simulations. Subsequently, the samples were irradiated with 2.2 GeV ^{197}Au ions at a fluence of 5×10^{10} ions cm^{-2} at the GSI Helmholtz Centre (Darmstadt, Germany) . The incident ion direction was normal to the polished surface, therefore leading to tracks parallel ($\parallel c$) for apatite and parallel, as well as perpendicular ($\perp c$), to the *c* axis for quartz. While the irradiation energy of 2.2 GeV by far exceeds those of typical fission fragments, the basic mechanism for track formation remains the same in both energy regimes (Afra *et al.*, 2011; Li *et al.*, 2012). The significantly longer track length associated with the higher energy enables more precise determination of the track radii by SAXS. We note that the electronic energy loss for 2.2 GeV is only less than a factor of two larger than that for natural fission fragments. For both energies, 2.2 GeV Au ions and the energy range of fission products (100 MeV), the ions interact nearly exclusively with the target's electrons; therefore, ion–nuclear interactions only account for 0.1% (2.2 GeV) and 1% (100 MeV), respectively, of the total energy loss.

Using a Boralectric heating element the irradiation temperature of one sample set was varied between RT and 913 K for quartz, and RT and 633 K for apatite. The temperature was directly measured at the specimen and PID (proportional-integral-derivative) controlled. For comparison, another set of samples was irradiated at room temperature and subsequently mounted on the same sample holder as the samples irradiated at high temperature (high-T) to make sure that these reference samples experience the same heating cycle. Depending on the annealing temperature, each sample was heated for between 8 and 15 min.

According to the SRIM-2008 data (http://www.srim.org/; Ziegler *et al.*, 1985), the range of 2.2 GeV Au ions is approximately 90 µm and the electronic energy losses (dE/dx) at the surface are 24 and 27 keV nm^{-1}, for quartz and apatite, respectively. The track formation threshold was reported to be 2 keV nm^{-1} for quartz (Klaumünzer, 2004) and 5 keV nm^{-1} for apatite (Tisserand *et al.*, 2004). To study the effect of temperatures below RT, two additional apatite samples of 30 µm thickness were irradiated at 23 K and RT with 1.7 GeV Au ions at a fluence of 7.5×10^{10} ions cm^{-2}.

For characterization of the track radii, small-angle X-ray scattering measurements were performed at the SAXS beamline at the Australian Synchrotron in Melbourne. The energy of the X-ray beams was 11 keV and the camera length was 1.6 m. The scattered intensity was collected using a Pilatus 1M detector with exposure times of 5 and 10 s. The spot size of the X-ray beam was approximately 0.04 mm^2. SAXS spectra were taken with tracks orientated parallel, as well as tilted by 5 and 10°, with respect to the X-ray beam. As demonstrated earlier, prolonged sample exposure to X-rays has no measureable effect on the track dimensions in apatite (Afra *et al.*, 2011). An unirradiated sample provided data for background removal. A more detailed description of SAXS measurements for ion track studies can be found elsewhere (Kluth, Schnohr, Pakarinen *et al.*, 2008; Afra *et al.*, 2011, 2013; Rodriguez *et al.*, 2012).

The measurements on quartz were complemented with calculations using MD simulations with temperature input from an inelastic thermal spike (i-TS) model. The MD calculations were performed with the *PARCAS24* (K. Nordlund, 2006, unpublished) code for a 25 nm cubic cell with periodic boundary conditions, containing 1.3 million atoms. The main principles of the MD algorithm are presented by Nordlund *et al.* (1998) and Ghaly *et al.* (1999). The adaptive time step and electronic stopping algorithms are the same as described by Nordlund (1995). The system resembles the ideal crystalline structure of quartz with the tracks aligned $\parallel c$. Prior to track creation, the simulation cell was heated to the temperature used in the experiment and subsequently relaxed. This takes the initial thermal expansion of the unit cell into account. During track simulation, 5 Å-thick border regions in the *x*- and *y*-axis directions were kept at the target temperature by a Berendsen temperature control (Berendsen *et al.*, 1984) to mimic heat conduction through the sample. The atomic interactions were calculated with the Watanabe–Samela Si—O mixed system many-body potential (Watanabe *et al.*, 2004; Samela *et al.*, 2008). The electronic energy loss of the track producing ions was 12.5 keV nm^{-1}. This energy deposition was implemented by continuously following the evolution of the atomic lattice temperature as calculated with the same i-TS model. It solves the energy-diffusion equations of the electron and atomic sublattice numerically and is explained in more detail by Afra *et al.* (2013). The temperature dependence of the electron–phonon coupling was neglected because, according to the i-TS calculations described by Dufour *et al.* (2012), the energy transfer between 300 and 900 K only decreases by 2.7%. Additionally the high-T irradiation effect was estimated for quartz by i-TS calculations (Toulemonde *et al.*, 2000) for 300 and 923 K.

3. Results and discussion

Scattering images of SAXS measurements for quartz irradiated at RT are shown in Fig. 1(*a*) and at high-T in Fig. 1(*b*).

Similar images for apatite are shown in Figs. 1(*c*) and 1(*d*). The intensity represents the scattering in q space, with dark colours corresponding to high scattering intensities. Under tilted geometry (Fig. 1), the scattering of ion tracks is highly anisotropic and characterized by two streaks with oscillating intensity. This pattern is caused by the high aspect ratio of the tracks up to 10 000. While the scattering intensities extracted from the streaks can only give information on the radial morphology of the ion tracks, the observed high anisotropy in the tilted images and the absence of scattering perpendicular to the streaks indicate continuous tracks. For both materials, similar streaky scattering patterns are observed from tracks created at RT to high-T, displaying similar track morphologies in both cases, *i.e.* long aspect ratio. Analysing the intensity within these streaks as a function of scattering vector yields information about the radial electron density of the tracks. The strong intensity oscillations indicate a sharp density transition between the track and the surrounding matrix. It should be noted that SAXS averages over a large number of tracks ($\sim 10^7$ for given beamsize and ion fluences in this work). However, the homoenergetic ion irradiation normal to the surface produces almost identical, parallel tracks and the information from the SAXS analysis can thus be related to the structure of 'individual' tracks.

Figs. 2(*a*)–2(*b*) show the scattering intensities (open circles) of ion tracks in quartz as a function of the scattering vector for different temperatures applied during irradiation. The tracks are aligned either $\parallel c$ (Fig. 2*a*) or $\perp c$ (Fig. 2*b*). The corresponding scattering intensities for apatite are presented in Fig. 2(*c*). The strong oscillations of the SAXS intensities indicate rather monodisperse track radii and a sharp density transition between the track and the matrix material. For both materials, the intensity minima shift towards lower q values with increasing irradiation temperature, which is a clear indication of increasing track radii. The best results in fitting the spectra were found using a cylinder model with a constant density. The form factor can be expressed as $f(q) = (2\pi LR\rho_0/q)J_1(Rq)$, where L is the track length, R the track radius, ρ_0 the density difference between track and matrix material, and $J_1(x)$ the Bessel function of first order. The scattering intensity is given by $I(q) \simeq |f(q)|^2$ (Engel *et al.* 2009). The track radius is convoluted with a narrow Gaussian distribution of width σ_r (Kluth, Schnohr, Pakarinen *et al.*, 2008; Rodriguez *et al.*, 2012), to account for a variation of the radius with depth within the sample (Li *et al.*, 2012). This parameter was typically found to be within the range of 0.2–0.4 nm (5–10% of R) for quartz and between 0.4 and 0.6 nm (8–11% of R) for apatite and corresponds approximately to the variation in track radius over the length of the track. The optimal fitting parameters were determined iteratively by a least-squares algorithm.

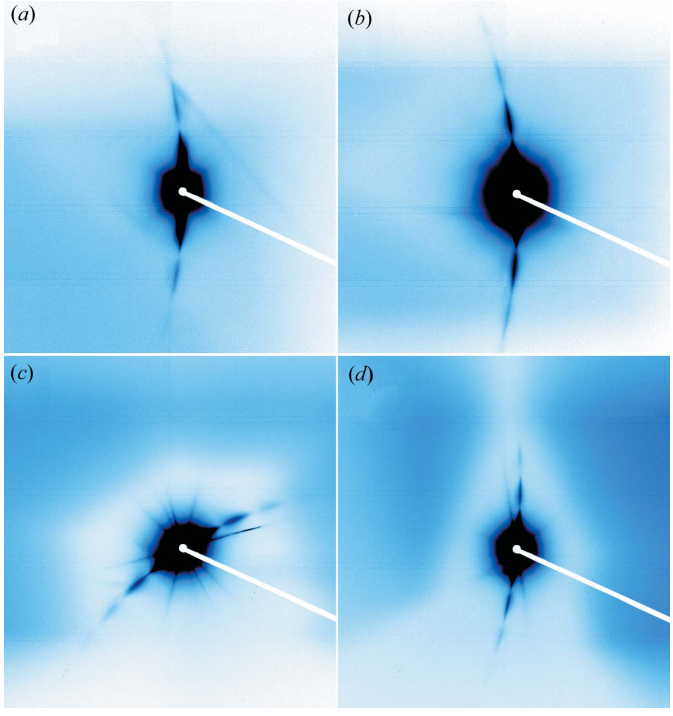

Figure 1
X-ray scattering images under 10° tilt for quartz irradiated at (*a*) RT and (*b*) 773 K, as well as for apatite irradiated at (*c*) RT and (*d*) 633 K. Although the track radius changes for both minerals, the track morphology and high aspect ratio does not seem to change from RT to high-T formed tracks.

Table 1
Radius increase for tracks exposed to elevated temperatures during irradiation.

The experimental values for quartz with two different track orientations and apatite are deduced from SAXS measurements; corresponding simulations are performed by MD and i-TS calculations.

Material (technique, track orientation)	High-T $\Delta R/\Delta T$ (nm per 100 K)	RT reference $\Delta R/\Delta T$ (nm per 100 K)
Quartz (SAXS, $\parallel c$)	0.06 (2)	0.02 (1)
Quartz (SAXS, $\perp c$)	0.08 (2)	0.02 (1)
Quartz (i-TS simulation)	0.07	–
Quartz (MD simulation, $\parallel c$)	0.10	–
Apatite (SAXS, $\parallel c$)	0.06 (1)	0.02 (1)

The fits to the model are shown as solid lines in Figs. 2(*a*)–2(*c*) and the track radii deduced from the fitting procedure are shown in Figs. 2(*d*)–2(*f*). The uncertainty due to the fitting routine is around 0.2%, whereas comparing SAXS measurements from different angles and exposure times yields a typical error for the track radius of 1% for quartz and 0.5% for apatite (see error bars in Fig. 2). Tracks in quartz show typical radii of 3.5–3.7 nm for RT irradiation, which is of similar magnitude to TEM measurements at comparable stopping powers (Afra *et al.*, 2013). For tracks in apatite a radius of 5.1 nm was observed, which is in good agreement with TEM measurements (Afra *et al.*, 2011; Li *et al.*, 2012). In both minerals, tracks produced at elevated irradiation temperatures increase approximately linearly in radius with comparable rates of 0.6 (2) nm per 100 K for apatite and 0.08 (2) nm per 100 K for quartz. Additionally, tracks $\parallel c$ in quartz show a 5% larger radius than those $\perp c$ because of the non-cubic nature of quartz. The origin of this difference is beyond the scope of this investigation and will be discussed elsewhere. Figs. 2(*d*)–2(*f*) also present data from the set of reference samples which

were irradiated at RT and subsequently underwent the identical heating cycle as samples irradiated at high-T. The track radii of all reference samples increase during this post-irradiation annealing process, yet at a rate of three to four times less than the high-T irradiated samples.

Results of the MD simulations for tracks in quartz are shown as filled triangles in Fig. 2(*d*). Table 1 lists the experimental results for the increase in track radius with increasing irradiation temperature, together with the rates calculated with MD simulations as well as the i-TS model. Using the i-TS model an increase of 0.07 nm per 100 K was calculated, while the MD simulations yield a relative increase of 0.10 nm per 100 K. The discrepancy is attributed to the potential not fully describing the complex phenomenon, which is probably affected by the melting point, thermal expansion and elastic properties of the potential, at least. Also the uncertainties in the energy deposition might affect the track size as a function of temperature. However, the increase is of comparable size for the experiment and simulation and clearly indicates that at elevated irradiation temperatures less energy is necessary to form a molten track. As a consequence, the radius around the ion trajectory where the temperature exceeds the melting temperature of the material increases, yielding larger track radii. Note, the absolute value for the track radius is signifi-

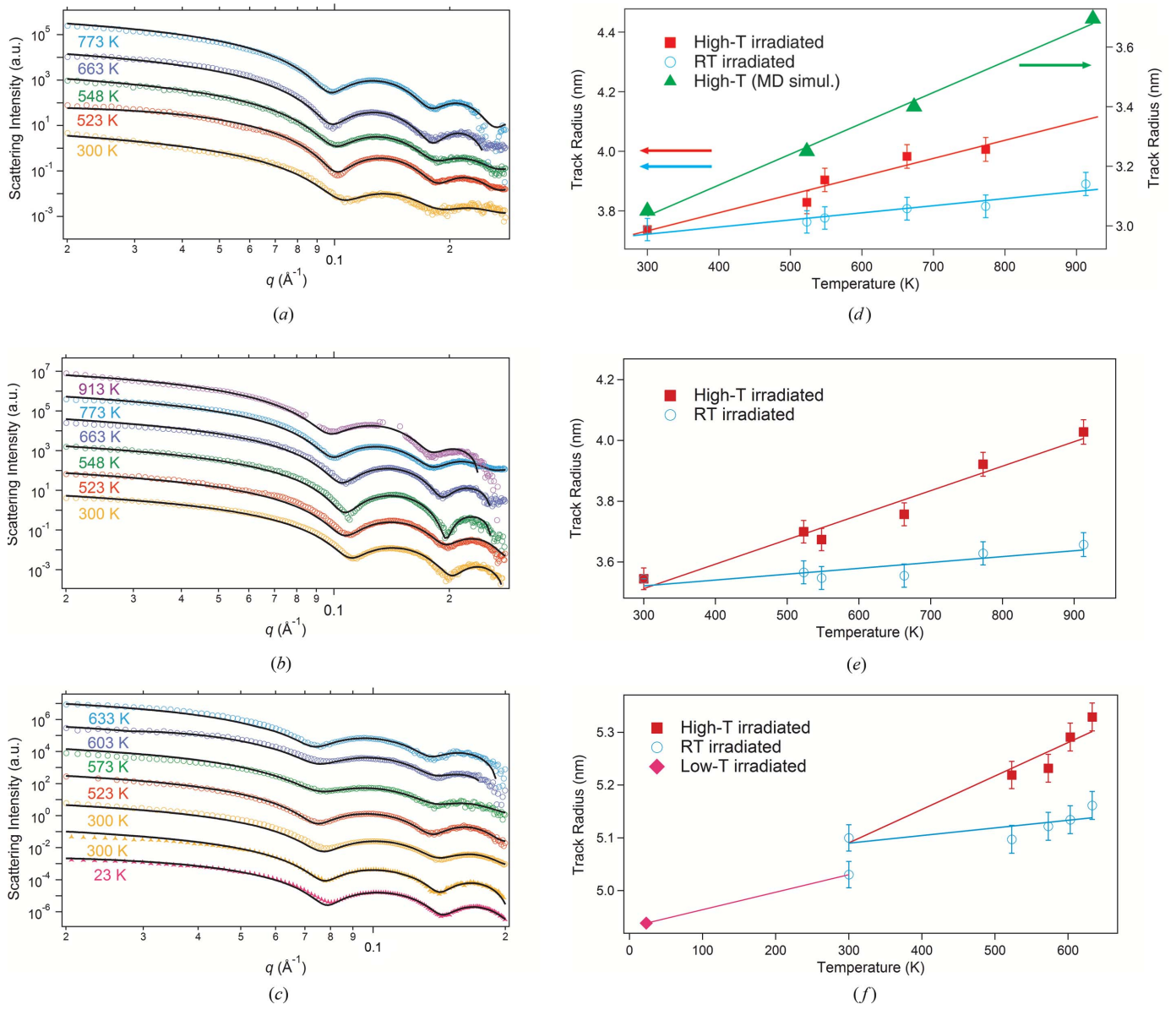

Figure 2
SAXS scattering intensities of ion tracks in quartz (*a*) ∥ *c* and (*b*) ⊥ *c* for different irradiation temperatures (open circles). (*c*) SAXS intensities for apatite ∥ *c* irradiated with 2.2 GeV (open circles) and 1.7 GeV (crosses) Au ions. A hard cylinder model was used to fit the results (solid lines). Spectra are offset for clarity. Typical intensity for each spectra at $q = 0$ is between 10 and 30 cm^{-1}. Track radius in quartz (*d*) ∥ *c* and (*e*) ⊥ *c* for high-T (filled squares) and the corresponding reference samples that underwent the same heat cycle (open circles). In (*d*) the right ordinate shows an MD simulation for ion tracks (filled triangles). Both vertical axes show the same scale. (*f*) Track radius in apatite ∥ *c* as a function of irradiation temperature for high-T (filled squares) and 23 K (filled diamonds) and as a function of annealing temperature for the reference samples (open circles).

cantly lower than measured. This offset is mainly a consequence of the simulation using an energy loss of only 12.5 keV nm^{-1} instead of the 24 keV nm^{-1} in the experiment.

The annealing of RT irradiated quartz reference samples also leads to an increase in the track radius at a rate of 0.02 (1) nm per 100 K. This is a factor of three to four below the growth rate observed for high-T irradiations. The effect is attributed to a heat-induced irreversible expansion of the ion tracks (B. Afra, 2013, unpublished). The increase of the track radius is linear over the entire temperature range tested, although above 846 K α-quartz undergoes a reversible phase transition into β-quartz with a change of the crystal structure from trigonal into hexagonal. The temperature effect on the track size appears to be unaltered by the phase transition.

For apatite, a relative increase of the radius by 0.06 (1) nm per 100 K irradiation temperature was found between RT and 633 K. The effect is quantitatively the same as for quartz and is also attributed to a reduced melting energy required to create a track at higher temperatures. An additional set of apatite samples, irradiated at 23 K and RT, also exhibits an increase with temperature at a rate of 0.03 nm per 100 K and therefore supports this explanation. The absolute radii of these two samples cannot be compared directly with the high-T series, as they were irradiated under slightly different conditions and possess different thicknesses. As in the case of quartz, annealing of RT irradiated apatite reference samples results in a much smaller size increase (approximately a factor of four) than the high-T irradiations. Although this behaviour appears similar to the observation in quartz, we ascribe the origin of the increasing track size to a generally different process. Annealing of existing tracks leads to a decrease in their size due to defect annealing and recrystallization processes at the track boundaries. For tracks in apatite, TEM investigations combined with *in situ* annealing describe in detail changes of the length, diameter and morphology of ion tracks upon annealing (Li *et al.*, 2012). The tracks 'disappear' first at the end, where the ion projectile stopped. Owing to the lower energy loss, the track size in this region is smaller and the damage less intensive, both providing better conditions for recovery processes. As SAXS measures an average over the whole track length, an initial damage recovery at the track end, *i.e.* where the track radius is small, leads to an apparent increase in the measured track radius.

The increase in track radii for both quartz and apatite was found to be significantly larger if irradiated under elevated temperatures than when simply annealed under the same conditions. This clearly suggests that enlarged tracks for high-T irradiation can be mainly attributed to the conditions during the track formation. In the framework of the present melt–quench process, which leaves a track consisting of amorphous material, a larger 'melting radius' yields an increased damage cross section upon resolidification. In contrast, for irradiation with low-energy ions in the keV to low MeV range, elevated temperatures generally lead to lower defect concentrations (Dhar et al., 1999). This is attributed to the thermally induced dynamic defect recovery. Previously, swift heavy-ion irradiation experiments have indicated irradiation induced recrystallization in apatite resulting in incomplete amorphization in the irradiated layer at high irradiation fluences (10^{13} ions cm^{-2}) (Miro et al., 2005). For the low fluences of 5×10^{10} ions cm^{-2} in this work, individual tracks covering about 4% of the surface area are formed. As such there is no proximity to the radiation on pre-existing amorphous damage and the effect of recrystallization is thus negligible. The density reduction results in a migration of atoms into the host crystal as well as on localized spots on the surface (Trautmann et al., 2002). Particular for quartz, this swelling effect leads to enhanced stress within the sample up to the destruction of the sample during the irradiation at higher fluences (Afra et al., 2013).

Absolute calibration of the scattering intensities provides an estimate of the density change between the host crystal and the ion tracks (Rodriguez *et al.*, 2012). Regardless of the irradiation temperature, values of $\rho_0 = 1.0\,(4)\%$ were obtained. The tracks in apatite showed a change of $\rho_0 = 0.6\,(3)\%$. Density changes of this magnitude are typical for amorphous tracks in these materials (Afra *et al.*, 2011, 2013).

Tracks in crystals exhibiting a strong ionic binding character, such as LiF (Schwartz *et al.*, 2001), also show a linear increase in damage cross section (0.04 nm per 100 K). While ion tracks in LiF are not found to be amorphous, but rather consist of discontinuous arrays of point-defect clusters (Trautmann *et al.*, 2000), this is an indication that the increase in damage radius with increasing temperature during formation is of general character for damage created by electronic energy loss such as that present during swift heavy-ion irradiation. In contrast to our observation of a constant density change, the density range in LiF decreases with increasing temperature, indicating that, while the damage cross section increases, the damage morphology (possibly point-defect density) decreases. This might be a result of competing processes of dynamic annealing and defect production.

To study if the damage recovery of the tracks in apatite is influenced by the formation temperature, we have performed *ex situ* annealing experiments with tracks generated at RT and 633 K. The track radius as a function of the annealing temperature is shown in Fig. 3. At each temperature point, the

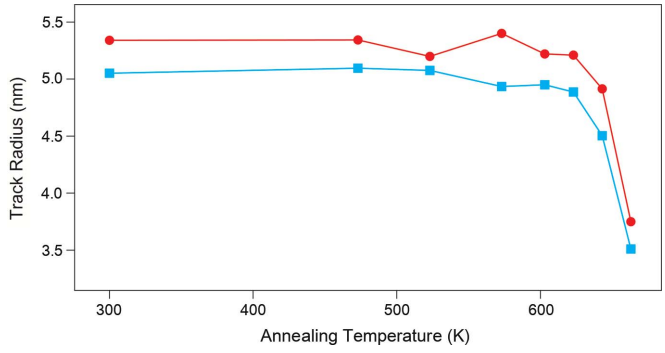

Figure 3
Ex situ annealing of tracks in apatite formed under 633 K (high-T, circles) and 300 K (RT, squares). At each temperature the samples were annealing for 20 min. The radius for both samples remains stable up to a temperature of 623 K.

samples were annealed for 20 min. For both samples the track radius remains approximately constant up to a temperature of 633 K, after which it drops rapidly until the tracks fade away shortly above 660 K. This behaviour is comparable to previous annealing experiments on apatite (Afra *et al.*, 2011). The absolute difference between tracks in these two samples remains nearly constant over the whole annealing temperature range. The similarity in annealing behaviour is one indication that tracks created under high-T do not differ in microstructure compared with those generated at RT. This may be relevant for application in fission track analysis, where the tracks are exposed to elevated temperatures over long periods of time. For RT-formed ion tracks in quartz a similar behaviour has been observed, with tracks being stable up to 1023 K (tracks $\parallel c$) and 823 K (tracks $\perp c$) after 2 h annealing (Sawamura *et al.*, 1999). No annealing experiments for tracks created in quartz under elevated temperatures are available.

4. Conclusion

We have used SAXS to characterize the radius of ion tracks in natural quartz and apatite that are formed at different irradiation temperatures. An increase in the track radii with increasing temperature was found. For quartz, both the MD simulations and the i-TS model show a similar increase. Results are consistent with a melt–quench process that is operational for track formation where the increased temperature reduces the energy required from the thermal spike to melt the material. An unaltered damage recovery behaviour upon post-irradiation annealing in apatite indicates no microstructural changes. Results suggest the increase in track radius is a general feature of swift heavy-ion irradiation. Our observations are in contrast to low-energy irradiation, where increased temperature during irradiation leads to a decrease in damage due to dynamic annealing.

The notion of increased track radii is particularly relevant for fission track dating, as naturally occurring tracks can be formed at elevated temperatures in the Earth's crust. Such changes are generally not considered and may result in different etched-track size distributions. Whether these findings can be applied to the length of ion tracks remains an open question.

This research was undertaken on the SAXS/WAXS beamline at the Australian Synchrotron. PK acknowledges the Australian Research Council for financial support. ML and RCE were supported by the Office of Basic Energy Sciences of the USDOE (DE-FG02-97ER45656). We thank M. Toulemonde for the i-TS calculations.

References

Afra, B., Lang, M., Rodriguez, M. D., Zhang, J., Giulian, R., Kirby, N., Ewing, R. C., Trautmann, C., Toulemonde, M. & Kluth, P. (2011). *Phys. Rev. B*, **83**, 064116.

Afra, B., Rodriguez, M. D., Trautmann, C., Pakarinen, O. H., Djurabekova, F., Nordlund, K., Bierschenk, T., Giulian, R., Ridgway, M. C., Rizza, G., Kirby, N., Toulemonde, M. & Kluth, P. (2013). *J. Phys. Condens. Matter*, **25**, 045006.

Berendsen, H. J. C., Postma, J. P. M., van Gunsteren, W. F., DiNola, A. & Haak, J. R. (1984). *J. Chem. Phys.* **81**, 3684–3690.

Bernet, M. & Garver, J. I. (2005). *Rev. Mineral. Geochem.* **58**, 205–237.

Dhar, S., Bolse, W. & Lieb, K.-P. (1999). *J. Appl. Phys.* **85**, 3120–3123.

Dufour, C., Khomenkov, V., Rizza, G. & Toulemonde, M. (2012). *J. Phys. D Appl. Phys.* **45**, 065302.

Engel, M., Stühn, B., Schneider, J. J., Cornelius, T. & Naumann, M. (2009). *Appl. Phys. A*, **97**, 99–108.

Gallagher, K., Brown, R. & Johnson, C. (1998). *Earth Planet. Sci. Lett.* **26**, 519–572.

Ghaly, M., Nordlund, K. & Averback, R. S. (1999). *Philos. Mag. A*, **79**, 795–820.

Gleadow, A., Duddy, I., Green, P. & Lovering, J. (1986). *Contrib. Mineral. Petrol.* **94**, 405–415.

Kamarou, A., Wesch, W., Wendler, E., Undisz, A. & Rettenmayr, M. (2006). *Phys. Rev. B*, **73**, 184107–184122.

Klaumünzer, S. (2004). *Nucl. Instrum. Methods Phys. Res. Sect. B*, **225**, 136–153.

Kluth, P., Schnohr, C. S., Pakarinen, O. H., Djurabekova, F., Sprouster, D. J., Giulian, R., Ridgway, M. C., Byrne, A. P., Trautmann, C., Cookson, D. J., Nordlund, K. & Toulemonde, M. (2008). *Phys. Rev. Lett.* **101**, 175503.

Kluth, P., Schnohr, C., Sprouster, D., Byrne, A., Cookson, D. & Ridgway, M. (2008). *Nucl. Instrum. Methods Phys. Res. Sect. B*, **266**, 2994–2997.

Li, W., Lang, M., Gleadow, A. J. W., Zdorovets, M. V. & Ewing, R. C. (2012). *Earth Planet. Sci. Lett.* **321**, 121–127.

Meftah, A., Brisard, F., Costantini, J. M., Dooryhee, E., Hage-Ali, M., Hervieu, M., Stoquert, J. P., Studer, F. & Toulemonde, M. (1994). *Phys. Rev. B*, **49**, 12457–12463.

Miro, S., Grebille, D., Chateigner, D., Pelloquin, D., Stoquert, J.-P., Grob, J.-J., Costantini, J.-M. & Studer, F. (2005). *Nucl. Instrum. Methods Phys. Res. Sect. B*, **227**, 306–318.

Nordlund, K. (1995). *Comput. Mater. Sci.* **3**, 448–456.

Nordlund, K., Ghaly, M., Averback, R. S., Caturla, M., de la Rubia, T. D. & Tarus, J. (1998). *Phys. Rev. B*, **57**, 7556–7570.

Paul, T. A. & Fitzgerald, P. G. (1992). *Am. Mineral.* **77**, 336–344.

Price, P. B. & Walker, R. M. (1962). *J. Appl. Phys.* **33**, 3407–3412.

Reiners, P. W. & Shuster, D. L. (2009). *Phys. Today*, **62**, 31–36.

Rodriguez, M., Afra, B., Trautmann, C., Toulemonde, M., Bierschenk, T., Leslie, J., Giulian, R., Kirby, N. & Kluth, P. (2012). *J. Non-Cryst. Solids*, **358**, 571–576.

Samela, J., Nordlund, K., Popok, V. N. & Campbell, E. E. B. (2008). *Phys. Rev. B*, **77**, 075309.

Sawamura, T., Baba, S. & Narita, M. (1999). *Radiat. Meas.* **30**, 453–459.

Schwartz, K., Benyagoub, A., Toulemonde, M. & Trautmann, C. (2001). *Radiat. Eff. Defects Solids*, **155**, 127–131.

Silk, E. C. H. & Barnes, R. S. (1959). *Philos. Mag.* **4**, 519–572.

Tisserand, R., Rebetez, M., Grivet, M., Bouffard, S., Benyagoub, A., Levesque, F. & Carpena, J. (2004). *Nucl. Instrum. Methods Phys. Res. Sect. B*, **215**, 129–136.

Toulemonde, M., Dufour, C., Meftah, A. & Paumier, E. (2000). *Nucl. Instrum. Methods Phys. Res. Sect. B*, **166**, 903–912.

Trautmann, C., Boccanfuso, M., Benyagoub, A., Klaumnzer, S., Schwartz, K. & Toulemonde, M. (2002). *Nucl. Instrum. Methods Phys. Res. Sect. B*, **191**, 144–148.

Trautmann, C., Toulemonde, M., Schwartz, K., Costantini, J. & Müller, A. (2000). *Nucl. Instrum. Methods Phys. Res. Sect. B*, **164**, 365–376.

Villa, F., Grivet, M., Rebetez, M., Dubois, C., Chambaudet, A., Chevarier, A., Martin, P., Brossard, P., Blondiaux, G., Sauvage, T. & Toulemonde, M. (1999). *Radiat. Meas.* **31**, 65–70.

Wagner, G. A. & Van den Haute, P. (1992). *Fission-Track Dating.* Dordrecht: Kluwer Academic Publishers.

Watanabe, T., Yamasaki, D., Tatsumura, K. & Ohdomari, I. (2004). *Appl. Surf. Sci.* **234**, 207–213.

Ziegler, J. F., Biersack, J. P. & Littmark, U. (1985). *The Stopping and Range of Ions in Matter.* New York: Pergamon.